Nonadiabatic Holonomic Quantum Computation Based on Rydberg Ground State Blockade

Shi-Lei Su(苏石磊), Chen Wang(王琛), P.-Y. Song(宋佩瑶), and Gang Chen(陈刚)*

School of Physics, Zhengzhou University, Zhengzhou 450001, China

(Received 2 January 2024; accepted manuscript online 18 March 2024)

Quantum gates are crucial for quantum computation and quantum information processing. However, their effectiveness is often hindered by systematic errors and decoherence. Therefore, achieving resilient quantum gates to these factors is of great significance. We present a method to construct nonadiabatic holonomic single- and two-qubit gates in a Rydberg ground-state-blockade regime. Our approach utilizes a far-off-resonant technique for the single-qubit gate and a modified Rydberg antiblockade for the two-qubit gate. The reduction of the population of single- and two-excitation Rydberg states and the nonadiabatic holonomic process during the construction of the gates ensure robustness to decoherence and systematic errors, respectively. Numerical results demonstrate the fidelity and robustness of our scheme. The proposed scheme holds promise for future applications in quantum computation and quantum information processing tasks.

DOI: 10.1088/0256-307X/41/4/040302

Rydberg atom, which owns long lifetime and hyperfine ground state energy levels, is a very appealing physical platform for quantum information processing.[1] The direct Rydberg–Rydberg interactions (RRI) between atoms, including the resonant dipole-dipole interaction scaling as $1/R^3$ and the van der Waals interaction scaling as $1/R^6$,[2–4] are the most important characteristic compared to other quantum platforms. Rydberg blockade[1–3,5–9] is one of the intriguing phenomena that arise from the RRI, which can suppress the simultaneous excitation of surrounding atoms when one atom has reached the high-lying Rydberg state. It was first applied in the construction of quantum logic gates by Jaksch *et al.*[6] Up to date, Rydberg blockade has facilitated lots of quantum gates and entanglement generation schemes.[10–17] On the contrary, the phenomenon of simultaneous excitation of Rydberg states under certain conditions is called Rydberg antiblockade (RAB),[18] which can also be realized by the RRI and allows the existence of two or more excited Rydberg atoms in a small spatial area. By adjusting the detuning between the driving field and atomic transition frequencies to make it satisfy some specific criteria, the energy shift induced by the Rydberg interaction can be compensated. Thus, the resonant transition between the Rydberg pair state and ground states is achieved. It offers yet another alternative method to build quantum gates.[19–23] Moreover, Rydberg dressing[24,25] and unconventional Rydberg pumping[26–28] caused by RRI have also been explored to realize quantum computation. Very recently, researchers proposed reconfigurable atom arrays[29] and parallel quantum entangling gates[30] on Rydberg atoms. Therefore, designing feasible quantum gates for these demonstrated quantum configurations is warranted.

The primary obstacles to achieving quantum computation are the inevitable decoherence of qubits and systematic errors. Geometric phase, with its inherent properties, is resilient to local systematic errors because it is insensitive to the evolution details but depends on the global path.[31–34] One of the well-known geometric phases is Berry phase discovered by Berry in 1984, also called adiabatic Abelian geometric phase since it is derived from adiabatic conditions.[31,35] However, the geometric quantum computation (GQC) based on adiabatic Abelian[31,36] or non-Abelian[32,37,38] requires longer evolution time to satisfy the adiabatic condition,[39] which results in a significant decline in the fidelity of the quantum system due to decoherence, and may even render the operation invalid. In response to this challenge, geometric quantum computation (GQC) has been proposed based on nonadiabatic Abelian[40–42] and non-Abelian[43–45] phases. The nonadiabatic non-Abelian approach, also known as nonadiabatic holonomic quantum computation (NHQC), avoids the long-time evolution requirements of adiabatic processes while maintaining robustness to systematic errors due to its geometric feature.[44,45]

Additionally, for quantum computation schemes that rely on excited states as ancillary states, the decay of the excited state undoubtedly leads to decoherence and increases the infidelity.[46] Experimentally, Zhou *et al.* have observed the ground-state geometric phase in the three-spin XY model.[47] The ground-state blockade has been observed[48] and designed to achieve a two-qubit quantum logic gate based on the Abelian geometric phase[49] as well as the quantum entanglement.[10] On that basis, to minimize the influence of the decay from excited states, to ensure the robustness of quantum computation to control errors, and further to explore the advantages of ground-state blockade schemes in multi-level systems, we utilize far-off-resonant couplings with excited states and construct effective Hamiltonians for single- and two-qubit cases,[14,19,50] based on which we realize the NHQC (including single- and two-qubit quantum logic gates) between ground states.

*Corresponding author. Email: chengang971@163.com
© 2024 Chinese Physical Society and IOP Publishing Ltd

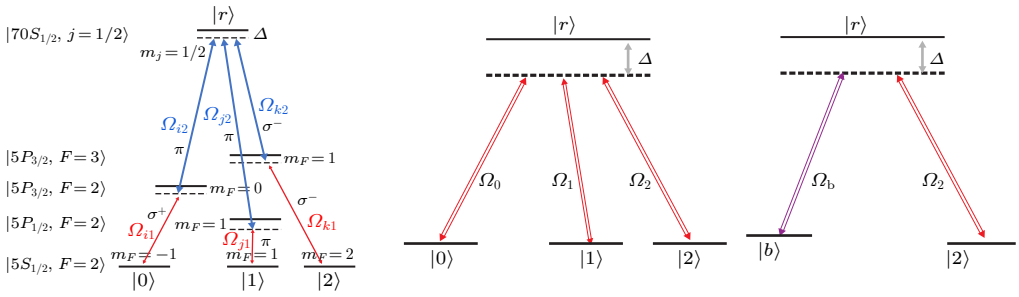

Fig. 1. Schematic diagrams of the single-qubit gate for (a) experimental, (b) simplified, and (c) secondary simplified energy levels, with the parameters defined in the text.

Single-Qubit Gate. As shown in Fig. 1(a), a Rydberg ^{87}Rb atom consists of three ground states $|0\rangle \equiv |5S_{1/2}, F=2, m_F=-1\rangle$, $|1\rangle \equiv |5S_{1/2}, F=2, m_F=1\rangle$, $|2\rangle \equiv |5S_{1/2}, F=2, m_F=2\rangle$, and a Rydberg state $|r\rangle \equiv |70S_{1/2}, j=2, m_j=1/2\rangle$, which are employed for the single-qubit gate. The ground states and the Rydberg state are far off resonance coupled by two-photon excitations, where $|0\rangle \leftrightarrow |r\rangle$ is driven by a σ^+-polarized laser Ω_{i1} at 780 nm and π-polarized one Ω_{i2} at 480 nm with intermediate state $|5P_{3/2}, F=2, m_F=0\rangle$, $|1\rangle \leftrightarrow |r\rangle$ is driven by a π-polarized laser Ω_{j1} at 795 nm and π-polarized one Ω_{j2} at 474 nm with intermediate state $|5P_{1/2}, F=2, m_F=1\rangle$, and $|2\rangle \leftrightarrow |r\rangle$ is driven by a σ^--polarized laser Ω_{k1} at 780 nm and σ^--polarized one Ω_{k2} at 480 nm with intermediate state $|5P_{1/2}, F=3, m_F=1\rangle$. The simplified model after adiabatic eliminating the intermediate states is shown in Fig. 1(b), the ground states $|k\rangle$ are driven by the laser $\Omega_k e^{i\varphi_k}$ with detuning Δ and $k=0, 1, 2$, where we assume $\varphi_2=0$ for convenience. The Hamiltonian of the system in the interaction picture is described by

$$H_1(t) = \frac{1}{2}(\Omega_0 e^{i\varphi_0}|r\rangle\langle 0| + \Omega_1 e^{i\varphi_1}|r\rangle\langle 1| + \Omega_2|r\rangle\langle 2|) + \text{H.c.} + \Delta|r\rangle\langle r|. \quad (1)$$

If we set $\Omega_b = \sqrt{\Omega_0^2+\Omega_1^2}$, $\Omega_0/\Omega_1 = \tan\theta/2$ with θ being a constant and $\varphi = \varphi_0 - \varphi_1$, Eq. (1) will be simplified to

$$H_1(t) = \frac{1}{2}(\Omega_b e^{i\varphi_1}|r\rangle\langle b| + \Omega_2|r\rangle\langle 2|) + \text{H.c.} + \Delta|r\rangle\langle r|, \quad (2)$$

with the bright state $|b\rangle = \sin(\theta/2)e^{i\varphi}|0\rangle + \cos(\theta/2)|1\rangle$, and a dark state $|d\rangle = \cos(\theta/2)|0\rangle - \sin(\theta/2)e^{-i\varphi}|1\rangle$ that is orthogonal to $|b\rangle$. The corresponding secondary simplified energy-level diagram is displayed in Fig. 1(c).

When $\Delta \gg \{\Omega_0, \Omega_1, \Omega_2\}$, we can obtain the effective Hamiltonian [51]

$$H_{1e}(t) = -\frac{\Omega_b\Omega_2}{4\Delta}|b\rangle\langle 2| + \text{H.c.} + \frac{\Omega_b^2+\Omega_2^2}{4\Delta}|r\rangle\langle r| - \frac{\Omega_b^2}{4\Delta}|b\rangle\langle b| - \frac{\Omega_2^2}{4\Delta}|2\rangle\langle 2|,$$

in which $\varphi_1 = 0$. The latter three terms are Stark shifts caused by large detuning conditions and can be eliminated by phase corrections [52,53] or auxiliary detuned transitions. [50,54–56] Consequently, the effective Hamiltonian is further simplified to

$$\mathcal{H}_{1e}(t) = -\frac{\Omega_b\Omega_2}{4\Delta}|b\rangle\langle 2| + \text{H.c.} \quad (3)$$

It can be easily demonstrated that Eq. (3) satisfies the conditions of NHQC. [44,45] Thus, it is determined that the scheme based on Eq. (3) owns the feature of holonomic quantum computation. The bright state $|b\rangle$ would achieve a π phase after cyclic evolution with time $T = 4\Delta\pi/\Omega_b\Omega_2$. The final evolution operator can be expressed as $U_1 = -|b\rangle\langle b| + |d\rangle\langle d| = \boldsymbol{n}\cdot\boldsymbol{\sigma}$ with $\boldsymbol{n} = (-\sin\theta\cos\varphi, \sin\theta\sin\varphi, \cos\theta)$, and $\boldsymbol{\sigma} = (\sigma_x, \sigma_y, \sigma_x)$ as the standard Pauli operator acting on $|0\rangle$ and $|1\rangle$. Here, the arbitrary holonomic gate can be constructed by selecting the parameters (θ, φ), such as $U_1(\pi/4, \pi)$ corresponds to the Hadamard gate while $U_1(\pi/2, \pi)$ corresponds to Pauli X.

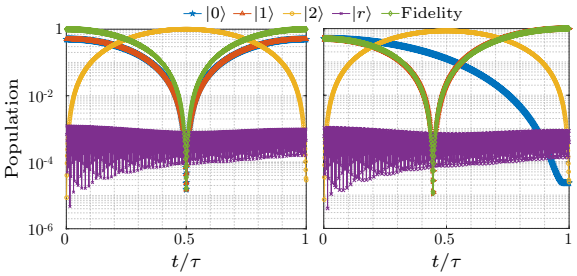

Fig. 2. Schematic diagrams of single-qubit gates X (left) and Hadamard (right), where $\Omega_2 = 2\pi \times 1$ MHz, $\Omega_b = \sqrt{2}\Omega_2$, and $\Delta = 40\Omega_2$.

The actual evolution of the system considering atomic decay is dominated by the Lindblad master equation

$$\dot{\rho}(t) = i[\rho(t), H(t)] + \frac{1}{2}\sum_j \Gamma_1\mathcal{L}(\sigma_j^-), \quad (4)$$

where the Lindblad operator is $\mathcal{L}(\mathcal{A}) = 2\mathcal{A}\rho(t)\mathcal{A}^\dagger - \mathcal{A}^\dagger\mathcal{A}\rho(t) - \rho(t)\mathcal{A}^\dagger\mathcal{A}$ with j denoting the jth atom. Here, the jth atom is associated with the operators $\sigma_j^- = (|0\rangle_j\langle r| + |1\rangle_j\langle r| + |2\rangle_j\langle r|)/\sqrt{3}$ which describe the system spontaneous emission. $H(t)$ is the total Hamiltonian of our scheme. Using the Alkali–Rydberg–Calculator, [57] the C_6 and decay rate of Rydberg state $|70S_{1/2}, j=2, m_j=1/2\rangle$ are evaluated as 86.30 GHz·μm^6 and 2.73 kHz at temperature 5.2 K, respectively. We numerically simulate the population and fidelity defined by $F = \langle\psi_f|\rho(t)|\psi_f\rangle$, where $|\psi_f\rangle = U_1(\theta, \varphi)|\psi(0)\rangle$ is the target state with the initial state $|\psi(0)\rangle$. The results of gates X and Hadamard are shown in Fig. 2 for $|\psi(0)\rangle = (|0\rangle - |1\rangle)/\sqrt{2}$. The population of Rydberg state $|r\rangle$ is always below 10^{-3}, while the population of state $|2\rangle$ approximately vanishes after cyclic evolution. The fidelities of gates X and Hadamard

arrive at 99.95% and 99.96%, respectively, and they can be further improved by increasing the detuning Δ.

In addition, our scheme is compatible with many platforms for four energy levels, and can be generalized to single-loop NHQC,[58] NHQC+,[59,60] and Brachistochrone NHQC[61–64] schemes. In the Supplementary Material, we take the Brachistochrone NHQC as an example to generalize our scheme.

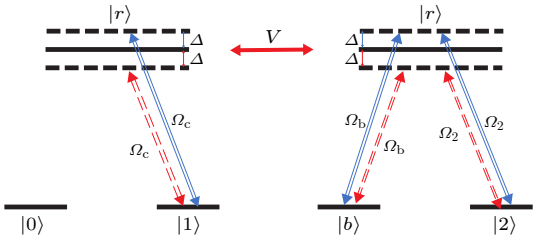

Fig. 3. Schematic diagrams of a two-qubit gate.

Two-Qubit Gate. We consider two identical atoms which are assigned as the control (left) atom and the target (right) atom as shown in Fig. 3. The control atom is exposed to two lasers with identical Rabi frequencies Ω_c and opposite red and blue detunings Δ, respectively, to couple $|1\rangle$ with $|r\rangle$. Meanwhile, the states $|b\rangle$ and $|2\rangle$ of the target atom are coupled to $|r\rangle$ by the lasers with Rabi frequencies Ω_b and Ω_2, respectively, mirroring the configuration in Fig. 1(c) but with two additional lasers with blue detunings. The purpose of using such lasers with opposite detunings is to remove the unnecessary Stark shifts during the dynamical process, which originates from auxiliary detuned transitions.[14,50,54] With the consideration of rotating-wave approximation and moving to the rotating frame, the Hamiltonian for the two-qubit system reads

$$H_2(t) = H_c(t) + H_t(t) + V|rr\rangle\langle rr|, \tag{5}$$

where

$$H_c(t) = \frac{1}{2}\Omega_c|r\rangle_1\langle 1|(e^{i\Delta t} + e^{-i\Delta t}) + \text{H.c.},$$
$$H_t(t) = \frac{1}{2}(\Omega_b|r\rangle_2\langle b| + \Omega_2|r\rangle_2\langle 2|)(e^{i\Delta t} + e^{-i\Delta t}) + \text{H.c.}$$

The terms $H_c(t)$ and $H_t(t)$ represent the Hamiltonians of the control and target Rydberg atoms, respectively. The Rydberg–Rydberg interaction is denoted by $V|rr\rangle\langle rr|$. Assuming $\Delta \gg \{\Omega_c, \Omega_b, \Omega_2\}$ and $V = 2\Delta$, the simplified form of $H_2(t)$ is given by

$$H_{2e}(t) = \frac{\Omega_c\Omega_b}{2\Delta}|rr\rangle\langle 1b| + \frac{\Omega_c\Omega_2}{2\Delta}|rr\rangle\langle 12| + \text{H.c.} + \frac{\Omega_c^2 + \Omega_b^2 + \Omega_2^2}{4\Delta}|rr\rangle\langle rr|$$

with $\varphi_1 = 0$. The two-atom ground states $\{|10\rangle, |11\rangle, |12\rangle\}$ can be resonantly excited to the Rydberg state $|rr\rangle$, a phenomenon known as Rydberg antiblockade. This enables the implementation of NHQC because $H_{2e}(t)$ takes the form of $\tilde{\Omega}|rr\rangle(\alpha\langle 1b| + \beta\langle 12|) + \text{H.c.}$, satisfying the parallel transportation and cyclic evolution conditions of NHQC.[44,45] However, the gate fidelity may be significantly affected by decay and interatomic distance fluctuations.[18,23,65,66] Therefore, we further modify the Rydberg antiblockade condition as $V - 2\Delta = V_0$, with V_0 being relatively smaller than $\{V, \Delta\}$, leading to a slightly different effective Hamiltonian.

$$H'_{2e}(t) = \Omega_{e1}|rr\rangle\langle 1b| + \Omega_{e2}|rr\rangle\langle 12| + \delta|rr\rangle\langle rr|, \tag{6}$$

where $\Omega_{e1} = \frac{\Omega_c\Omega_b}{2\Delta}$, $\Omega_{e2} = \frac{\Omega_c\Omega_2}{2\Delta}$, and $\delta = V_0 + \frac{\Omega_c^2+\Omega_b^2+\Omega_2^2}{4\Delta}$ (see the Supplementary Material for detailed derivation). From Eq. (6), the condition $\delta \gg \{\Omega_{e1}, \Omega_{e2}\}$ leads to the effective Hamiltonian

$$\mathcal{H}_{2e} = -\frac{\Omega_{e2}\Omega_{e1}}{\delta}|1b\rangle\langle 12| + \text{H.c.}, \tag{7}$$

which enables the realization of NHQC. After a period $T = \pi\delta/(\Omega_{e2}\Omega_{e1})$, the state $|b\rangle$ of the target atom acquires a π geometric phase. The evolution operation can be expressed as $U_2(\theta, \varphi) = |0b\rangle\langle 0b| + |0d\rangle\langle 0d| + |1d\rangle\langle 1d| - |1b\rangle\langle 1b|$. The fidelity of a general gate $U_2(\pi/2, \pi)$ by using a simple initial state $|\psi(0)\rangle = (|00\rangle + |01\rangle + |10\rangle - |11\rangle)/2$ is evaluated using the Schrödinger equation $i\frac{d}{dt}|\psi(t)\rangle = H(t)|\psi(t)\rangle$ with the initial Hamiltonian. The result, shown in Fig. 4, indicates that the fidelity exceeds 99% over a large parameter range (the fidelity is used as $|\langle\psi_f|U_2(\pi/2, \pi)|\psi(0)\rangle|^2$ here, where $|\psi_f\rangle$ denotes the final state), reaching over 99.5% within $V_0/\Omega_c \in [1, 3]$ and $\Delta/\Omega_c \in [15, 35]$, which shows great robustness in contrast to the conventional Rydberg antiblockade regime.[20] Experimentally, the target atom can be illuminated similar to the single-qubit scheme, while the control atom can be driven by $\{\Omega_{k1}, \Omega_{k2}\}$ with an intermediate state $|5P_{1/2}, F = 3, m_F = 1\rangle$. In pursuit of generality, an arbitrary initial state is chosen as $|\psi'(0)\rangle = (\cos\Theta_1|0\rangle + \sin\Theta_1|1\rangle) \otimes (\cos\Theta_2|0\rangle + \sin\Theta_2|1\rangle)$ with $\{\Theta_1, \Theta_2\} \in [0, \pi]$ in the following numerical results and the average fidelity is defined as $\bar{F} = (1/\pi^2)\int\int|\langle\psi'(0)|\hat{U}_{id}^{+}|\psi'_f\rangle|^2 d\Theta_1 d\Theta_2$ with $\hat{U}_{id}$ and $|\psi'_f\rangle$ as the ideal two-qubit quantum gate and the final state respectively, which is the generalization of the average fidelity definition in Ref. [67]. The interaction between two Rydberg states $|70S_{1/2}, j = 2, m_j = 1/2\rangle$ is achieved at $2\pi \times 88.64$ MHz when the inter-atomic distance is 3.15 μm, and considering $U_2(\theta \in [0, \pi], \varphi = \pi)$, the fidelity is described in Fig. 5. It is observed that the final fidelity is 99.71% for the middle (green) line, corresponding to the CNOT gate $U_2(\pi/2, \pi)$, and the fidelity is close to 99.65% for the gate corresponding to $\theta = \pi$.

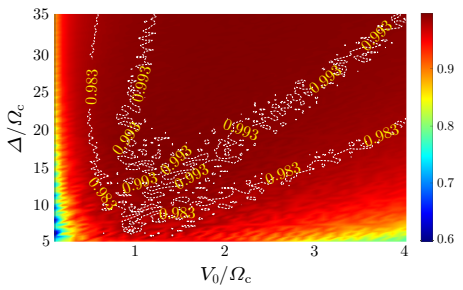

Fig. 4. Schematic diagrams of the fidelity of gate CNOT $U_2(\pi/2, \pi)$ against parameters Δ and V_0. Here the parameters are set as $\Omega_2 = \Omega_c$, $\Omega = \sqrt{2}\Omega_c$, in which we set the initial state as $|\psi(0)\rangle = (|00\rangle + |01\rangle + |10\rangle - |11\rangle)/2$.

For Rydberg antiblockade, the error from the interatomic distance is an important reason for the existence

of infidelity. Thus, we discuss the fluctuation range of the average fidelity based on modified Rydberg antiblockade. When we consider the random fluctuations, the corresponding Rydberg interaction can be written as $V' = V + F(t)$, where $F(t)$ is uniformly distributed over the interval $[-a, a]$ that is affected by atomic distance δr caused by atomic random motion. We set $F(t)/2\pi = -a + 2a\xi(t)$ MHz, in which $\xi(t)$ is a uniformly distributed random number in the interval [0, 1].[68] Assuming $a = 5$ that corresponds to $\delta r \approx 0.03\,\mu$m, and averaging the results after repeating numerical simulation of this stochastic process 100 times as shown in Fig. 6. Compared with Fig. 5 (the middle green line), the average fidelity under atomic random motion within 0.03 μm can still arrive at 99.68%. Thus, the fluctuation of inter-atomic distance within a small range randomly does not influence the average fidelity since the population of state $|rr\rangle$ almost has no occupation throughout as shown in Fig. 6.

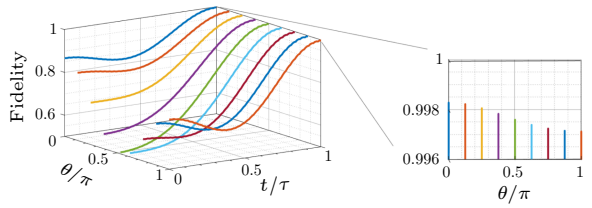

Fig. 5. Schematic diagrams of the fidelity against parameters θ with a range $[0, \pi]$. The left picture shows the time evolutions with different θ. The small picture on the right shows the θ–fidelity view. At this point, the parameters are set as $\Omega_c = \Omega_2 = 2\pi \times 2$ MHz, $\Omega_b = \sqrt{2}\Omega_c$, $\Delta = 22.42\Omega_c$, and $V_0 = 1.48\Omega_c$. The initial state is $|\psi'(0)\rangle = (\cos\Theta_1|0\rangle + \sin\Theta_1|1\rangle)\otimes(\cos\Theta_2|0\rangle + \sin\Theta_2|1\rangle)$.

Another significant error to be considered is the dephasing process,[69–71] which can be regarded as the average result of the laser phase noise $\Omega_i(t) = \Omega_i e^{i\phi_i(t)}$, where ϕ_i is the random process related to power spectral density $S_\phi(f)$ with f being phase-modulated Fourier frequency.[72,73] Here, we consider a suitable range by the experimental expectation $\Gamma_z \in [0, 2]$ kHz. The master equation after considering spontaneous emission and dephasing can be expressed as

$$\dot{\rho}(t) = i[\rho(t), H(t)] + \frac{1}{2}\sum_j [\Gamma_1 \mathcal{L}(\sigma_j^-) + \Gamma_2 \mathcal{L}(\sigma_j^z)], \quad (8)$$

where $\sigma_j^z = |0\rangle_j\langle 0| + |1\rangle_j\langle 1| + |2\rangle_j\langle 2| - |r\rangle_j\langle r|$. The result of numerical simulations is shown in Fig. 7. We can find that the fidelity decreases approximately linearly with the increase of dephasing within a certain small range, while the fidelity is still above 99% when $\Gamma_z = 2$ kHz. On the other hand, there are also some schemes to suppress the dephasing that can be specifically applied in experiments[74,75] to further improve the performance.

In a relevant paper,[46] decoherence-suppressed nonadiabatic holonomic quantum computation scheme is proposed, which can greatly suppress the population of the excited state so that it is of inherent robustness to the system decay. We can compare this scheme and the scheme in the relevant paper. Firstly, the present work makes use of an effective model to realize the nonadiabatic holonomic quantum computation in a four-level Rydberg atom system. However, the relevant paper uses a three-level nitrogen-vacancy center system to realize. Secondly, the present work mitigates the cyclic evolution condition while the relevant paper needs a strict cyclic evolution condition through setting the specific angle relation. Thirdly, for the construction of the single-qubit model, the present work nicely achieves the ground state blockade mechanism while the relevant paper still has the couplings between the ground states and the excited states.

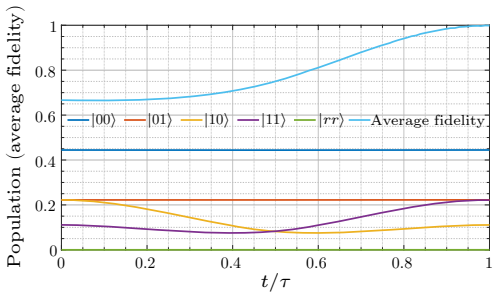

Fig. 6. Schematic diagrams of the populations of different bases including $\{|00\rangle, |01\rangle, |10\rangle, |11\rangle, |rr\rangle\}$ and average fidelity with the initial state $|\psi'(0)\rangle = (\cos\Theta_1|0\rangle + \sin\Theta_1|1\rangle)\otimes(\cos\Theta_2|0\rangle + \sin\Theta_2|1\rangle)$ for the gate $U_2(\pi/2, \pi)$, where the Rydberg interaction is set with random fluctuations corresponding atomic random motion $\delta r \approx 0.03\,\mu$m.

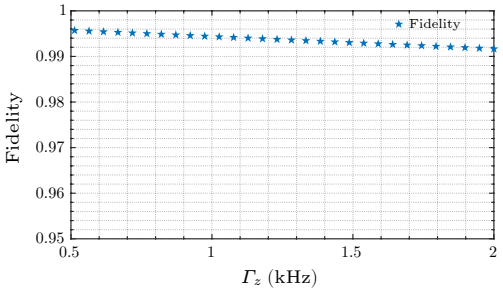

Fig. 7. Schematic diagrams of the fidelity for $U_2(\pi/2, \pi)$ against the dephasing rate Γ_z with a range [0.5,2] kHz. The parameters are set as $\Omega_c = \Omega_2 = 2\pi \times 2$ MHz, $\Omega_b = \sqrt{2}\Omega_c$, $\Delta = 22.42\Omega_c$, and $V_0 = 1.48\Omega_c$. The initial state is $|\psi'(0)\rangle = (\cos\Theta_1|0\rangle + \sin\Theta_1|1\rangle)\otimes(\cos\Theta_2|0\rangle + \sin\Theta_2|1\rangle)$.

In conclusion, we propose a scheme to realize nonadiabatic holonomic quantum computation based on Rydberg ground-state blockade. The large detuning is applied for a single-atom scheme while the two-atom one uses a modified Rydberg antiblockade. The Stark shift generated during the gate process can be eliminated using auxiliary detuned transitions, and we use two lasers with the same Rabi frequencies and opposite detunings to avoid the complex Stark shifts in a two-qubit scheme. The numerical results show the population of single Rydberg state in single-qubit and two Rydberg states in two-qubit schemes are less than 0.9%, which demonstrates the insensitivity of our scheme against atomic decay, the fluctuations of the RRI induced by the variations of inter-atomic distance, as well as the dephasing noise induced by two-excitation Rydberg states. Our scheme provides another perspective for the realization of nonadiabatic holonomic quantum com-

putation by adiabatically eliminating the excited states, which may open the mind of researchers in theories and experiments.

Acknowledgement. This work was supported by the National Natural Science Foundation of China (Grant No. 12274376).

References

[1] Gallagher T F 1984 *Rydberg Atoms* (Cambridge: Cambridge University Press)
[2] Saffman M, Walker T G, and Mølmer K 2010 *Rev. Mod. Phys.* **82** 2313
[3] Saffman M 2016 *J. Phys. B* **49** 202001
[4] Shi X F 2022 *Quantum Sci. Technol.* **7** 023002
[5] Urban E, Johnson T A, Henage T, Isenhower L, Yavuz D D, Walker T G, and Saffman M 2009 *Nat. Phys.* **5** 110
[6] Jaksch D, Cirac J I, Zoller P, Rolston S L, Côté R, and Lukin M D 2000 *Phys. Rev. Lett.* **85** 2208
[7] Shi X F 2018 *Phys. Rev. Appl.* **10** 034006
[8] Shi X F and Kennedy T A B 2017 *Phys. Rev. A* **95** 043429
[9] Gaëtan A, Miroshnychenko Y, Wilk T, Chotia A, Viteau M, Comparat D, Pillet P, Browaeys A, and Grangier P 2009 *Nat. Phys.* **5** 115
[10] Shao X Q, Li D X, Ji Y Q, Wu J H, and Yi X X 2017 *Phys. Rev. A* **96** 012328
[11] Liu Y Y, Sun Y, Fu Z, Xu P, Wang X, He X D, Wang J, and Zhan M S 2021 *Phys. Rev. Appl.* **15** 054020
[12] Shi X F 2019 *Phys. Rev. Appl.* **11** 044035
[13] Liu B J, Su S L, and Yung M H 2020 *Phys. Rev. Res.* **2** 043130
[14] Wu J L, Wang Y, Han J X, Su S L, Xia Y, Jiang Y, and Song J 2021 *Front. Phys.* **17** 22501
[15] Shi X F 2017 *Phys. Rev. Appl.* **7** 064017
[16] Zhao P Z, Cui X D, Xu G F, Sjöqvist E, and Tong D M 2017 *Phys. Rev. A* **96** 052316
[17] Zheng R H, Su S L, Song J, Li W, and Xia Y 2017 *Phys. Rev. A* **108** 042405
[18] Ates C, Pohl T, Pattard T, and Rost J M 2007 *Phys. Rev. Lett.* **98** 023002
[19] Su S L, Tian Y Z, Shen H Z, Zang H P, Liang E J, and Zhang S 2017 *Phys. Rev. A* **96** 042335
[20] Su S L, Gao Y, Liang E, and Zhang S 2017 *Phys. Rev. A* **95** 022319
[21] Wu J L, Wang Y, Han J X, Jiang Y, Song J, Xia Y, Su S L, and Li W 2021 *Phys. Rev. Appl.* **16** 064031
[22] Su S L, Shen H Z, Liang E, and Zhang S 2018 *Phys. Rev. A* **98** 032306
[23] Su S L, Guo F Q, Tian L, Zhu X Y, Yan L L, Liang E J, and Feng M 2020 *Phys. Rev. A* **101** 012347
[24] Bouchoule I and Mølmer K 2002 *Phys. Rev. A* **65** 041803
[25] Pupillo G, Micheli A, Boninsegni M, Lesanovsky I, and Zoller P 2010 *Phys. Rev. Lett.* **104** 223002
[26] Li D X and Shao X Q 2018 *Phys. Rev. A* **98** 062338
[27] Yin H D and Shao X Q 2021 *Opt. Lett.* **46** 2541
[28] Shao X Q 2020 *Phys. Rev. A* **102** 053118
[29] Bluvstein D, Evered S J, Geim A A *et al.* 2023 *Nature* **626** 58
[30] Evered S J, Bluvstein D, Kalinowski M *et al.* 2023 *Nature* **622** 268
[31] Berry M V 1984 *Proc. R. Soc. Lond. A* **392** 45
[32] Wilczek F and Zee A 1984 *Phys. Rev. Lett.* **52** 2111
[33] Zhang J, Kyaw T H, Filipp S, Kwek L C, Sjöqvist E, and Tong D M 2023 *Phys. Rep.* **1027** 1
[34] Guo A L, Tu T, Zhu L T, and Li C F 2021 *Chin. Phys. Lett.* **38** 094203
[35] Liu L J, Liu Y Z, and Tong D M 2009 *Chin. Phys. Lett.* **26** 030302
[36] Jones J A, Vedral V, Ekert A, and Castagnoli G 2000 *Nature* **403** 869
[37] Zanardi P and Rasetti M 1999 *Phys. Lett. A* **264** 94
[38] Duan L M, Cirac J I, and Zoller P 2001 *Science* **292** 1695
[39] Tong D M 2010 *Phys. Rev. Lett.* **104** 120401
[40] Aharonov Y and Anandan J 1987 *Phys. Rev. Lett.* **58** 1593
[41] Wang X B and Matsumoto K J 2001 *Phys. Rev. Lett.* **87** 097901
[42] Zhu S L and Wang Z D 2002 *Phys. Rev. Lett.* **89** 097902
[43] Anandan J 1988 *Phys. Lett. A* **133** 171
[44] Xu G F, Zhang J, Tong D M, Sjöqvist E, and Kwek L C 2012 *Phys. Rev. Lett.* **109** 170501
[45] Sjöqvist E, Tong D M, Andersson L M, Hessmo B, Johansson M, and Singh K 2012 *New J. Phys.* **14** 103035
[46] Liu B J, Yan L L, Zhang Y, Yung M H, Su S L, and Shan C X 2023 *Phys. Rev. Res.* **5** 013059
[47] Zhou H, Li Z K, Wang H Y, Chen H W, Peng X H, and Du J F 2016 *Chin. Phys. Lett.* **33** 060301
[48] Jau Y Y, Hankin A M, Keating T, Deutsch I H, and Biedermann G W 2016 *Nat. Phys.* **12** 71
[49] Xu J Z, Sun L N, Wei J F, Du Y L, Luo R H, Yan L L, Feng M, and Su S L 2022 *Chin. Phys. Lett.* **39** 090301
[50] Zhao Y J, Liu B, Ji Y Q, Tang S Q, and Shao X Q 2017 *Sci. Rep.* **7** 16489
[51] James D F and Jerke J 2007 *Can. J. Phys.* **85** 625
[52] Vepsäläinen A, Danilin S, and Paraoanu G S 2018 *Quantum Sci. Technol.* **3** 024006
[53] Vepsäläinen A, Danilin S, and Paraoanu G S 2019 *Sci. Adv.* **5** eaau5999
[54] Su S L, Liang E, Zhang S, Wen J J, Sun L L, Jin Z, and Zhu A D 2016 *Phys. Rev. A* **93** 012306
[55] Wang C, Han J X, Wu J L, Wang Y, Jiang Y, Xia Y, and Song J 2020 *Laser Phys.* **30** 045201
[56] Han J X, Wu J L, Wang Y, Jiang Y Y, Xia Y, and Song J 2020 *Opt. Express* **28** 1954
[57] Robertson E J, Šibalić N, Potvliege R M, and Jones M P A 2021 *Comput. Phys. Commun.* **261** 107814
[58] Herterich E and Sjöqvist E 2016 *Phys. Rev. A* **94** 052310
[59] Liu B J, Song X K, Xue Z Y, Wang X, and Yung M H 2019 *Phys. Rev. Lett.* **123** 100501
[60] Li M, Guo F Q, Jin Z, Yan L L, Liang E J, and Su S L 2021 *Phys. Rev. A* **103** 062607
[61] Liu B J, Xue Z Y and Yung M H 2020 arxiv:2001.05182[quant-ph]
[62] Wei J F, Guo F Q, Wang D Y, Jia Y, Yan L L, Feng M, and Su S L 2022 *Phys. Rev. A* **105** 042404
[63] Sun L N, Yan L L, Su S L, and Jia Y 2021 *Phys. Rev. Appl.* **16** 064040
[64] Dong Y, Feng C, Zheng Y, Chen X D, Guo G C, and Sun F W 2021 *Phys. Rev. Res.* **3** 043177
[65] Fu Z, Xu P, Sun Y, Liu Y Y, He X D, Li X, Liu M, Li R B, Wang J, Liu L, and Zhan M S 2022 *Phys. Rev. A* **105** 042430
[66] Su S L and Li W B 2021 *Phys. Rev. A* **104** 033716
[67] Zhu S L and Zanardi P 2005 *Phys. Rev. A* **72** 020301
[68] Li X X, You J B, Shao X Q, and Li W B 2022 *Phys. Rev. A* **105** 032417
[69] Tamura H, Yamakoshi T, and Nakagawa K 2020 *Phys. Rev. A* **101** 043421
[70] Madjarov I S, Covey J P, Shaw A L, Choi J, Kale A, Cooper A, Pichler H, Schkolnik V, Williams J R, and Endres M 2020 *Nat. Phys.* **16** 857
[71] Li X X, Shao X Q, and Li W B 2022 *Phys. Rev. Appl.* **18** 044042
[72] de Léséleuc S, Barredo D, Lienhard V, Browaeys A, and Lahaye T 2018 *Phys. Rev. A* **97** 053803
[73] Lee W, Kim M, Jo H, Song Y, and Ahn J 2019 *Phys. Rev. A* **99** 043404
[74] Shi X F 2020 *Phys. Rev. Appl.* **13** 024008
[75] Wang Y M, Su Y, Chen X, and Wu C F 2020 *Phys. Rev. Appl.* **14** 044043